Monthly Notices
of the
ROYAL ASTRONOMICAL SOCIETY

Mon. Not. R. Astron. Soc. **404,** 86–100 (2010) doi:10.1111/j.1365-2966.2010.16282.x

Galaxy And Mass Assembly (GAMA): the input catalogue and star–galaxy separation

I. K. Baldry,[1⋆] A. S. G. Robotham,[2] D. T. Hill,[2] S. P. Driver,[2] J. Liske,[3] P. Norberg,[4] S. P. Bamford,[5] A. M. Hopkins,[6] J. Loveday,[7] J. A. Peacock,[4] E. Cameron,[2,8] S. M. Croom,[9] N. J. G. Cross,[4] I. F. Doyle,[10] S. Dye,[11] C. S. Frenk,[12] D. H. Jones,[6] E. van Kampen,[3] L. S. Kelvin,[2] R. C. Nichol,[10] H. R. Parkinson,[4] C. C. Popescu,[13] M. Prescott,[1] R. G. Sharp,[6] W. J. Sutherland,[14] D. Thomas[10] and R. J. Tuffs[15]

[1]*Astrophysics Research Institute, Liverpool John Moores University, Twelve Quays House, Egerton Wharf, Birkenhead CH41 1LD*
[2]*Scottish Universities' Physics Alliance (SUPA), School of Physics and Astronomy, University of St Andrews, North Haugh, St Andrews, Fife KY16 9SS*
[3]*European Southern Observatory, Karl-Schwarzschild-Str. 2, 85748 Garching, Germany*
[4]*SUPA, Institute for Astronomy, University of Edinburgh, Royal Observatory, Blackford Hill, Edinburgh EH9 3HJ*
[5]*Centre for Astronomy and Particle Theory, University of Nottingham, University Park, Nottingham NG7 2RD*
[6]*Anglo Australian Observatory, PO Box 296, Epping, NSW 1710, Australia*
[7]*Astronomy Centre, University of Sussex, Falmer, Brighton BN1 9QH*
[8]*Department of Physics, Swiss Federal Institute of Technology (ETH-Zürich), CH-8093 Zürich, Switzerland*
[9]*Sydney Institute for Astronomy, School of Physics, University of Sydney, NSW 2006, Australia*
[10]*Institute of Cosmology and Gravitation (ICG), University of Portsmouth, Dennis Sciama Building, Burnaby Road, Portsmouth PO1 3FX*
[11]*School of Physics & Astronomy, Cardiff University, Queens Buildings, The Parade, Cardiff CF24 3AA*
[12]*Institute for Computational Cosmology, Department of Physics, Durham University, South Road, Durham DH1 3LE*
[13]*Jeremiah Horrocks Institute, University of Central Lancashire, Preston PR1 2HE*
[14]*Astronomy Unit, Queen Mary University London, Mile End Rd, London E1 4NS*
[15]*Max Planck Institute for Nuclear Physics (MPIK), Saupfercheckweg 1, D-69117 Heidelberg, Germany*

Accepted 2010 January 4. Received 2009 December 17; in original form 2009 September 24

ABSTRACT

We describe the spectroscopic target selection for the Galaxy And Mass Assembly (GAMA) survey. The input catalogue is drawn from the Sloan Digital Sky Survey (SDSS) and UKIRT Infrared Deep Sky Survey (UKIDSS). The initial aim is to measure redshifts for galaxies in three $4^\circ \times 12^\circ$ regions at 9, 12 and 14.5 h, on the celestial equator, with magnitude selections $r < 19.4, z < 18.2$ and $K_{\rm AB} < 17.6$ over all three regions, and $r < 19.8$ in the 12-h region. The target density is $1080\,{\rm deg}^{-2}$ in the 12-h region and $720\,{\rm deg}^{-2}$ in the other regions. The average GAMA target density and area are compared with completed and ongoing galaxy redshift surveys. The GAMA survey implements a highly complete star–galaxy separation that jointly uses an intensity-profile separator ($\Delta_{\rm sg} = r_{\rm psf} - r_{\rm model}$ as per the SDSS) and a colour separator. The colour separator is defined as $\Delta_{\rm sg,jk} = J - K - f(g - i)$, where $f(g - i)$ is a quadratic fit to the $J - K$ colour of the stellar locus over the range $0.3 < g - i < 2.3$. All galaxy populations investigated are well separated with $\Delta_{\rm sg,jk} > 0.2$. From 2 yr out of a 3-yr AAOmega program on the Anglo-Australian Telescope, we have obtained 79 599 unique galaxy redshifts. Previously known redshifts in the GAMA region bring the total up to 98 497. The median galaxy redshift is 0.2 with 99 per cent at $z < 0.5$. We present some of the global statistical properties of the survey, including K-band galaxy counts, colour–redshift relations and preliminary $n(z)$.

Key words: catalogues – surveys – galaxies: distances and redshifts – galaxies: photometry.

1 INTRODUCTION

Galaxy redshift surveys provide a fundamental resource for studies of galaxy evolution. The redshift of a galaxy can be used to obtain a distance assuming a set of cosmological parameters, modulo

⋆E-mail: ikb@astro.livjm.ac.uk

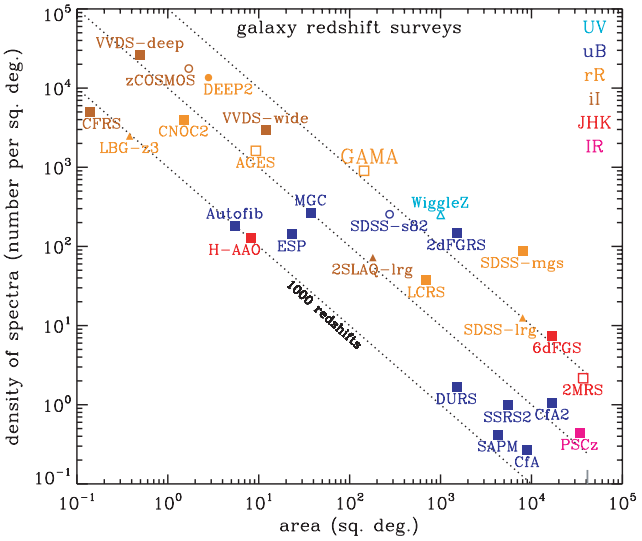

Figure 1. Comparison between field galaxy surveys with spectroscopic redshifts: squares represent predominantly magnitude-limited surveys; circles represent surveys involving colour cuts for photometric redshift selection; while triangles represent highly targeted surveys. The colours represent different principal wavelength selections as in the legend. Filled symbols represent completed surveys. See Table 1 for survey names and references.

peculiar velocities, and a well-defined selection function enables the comoving number density of galaxies to be estimated as a function of various properties e.g. galaxy luminosity functions (Schechter 1976; Binggeli, Sandage & Tammann 1988; Norberg et al. 2002b; Blanton et al. 2003). In addition, using the combined sky distribution and distance information, the clustering properties of galaxies can be determined (Davis, Geller & Huchra 1978; de Lapparent, Geller & Huchra 1988; Norberg et al. 2002a; Zehavi et al. 2005) and the velocity dispersion of galaxies in groups and clusters can be used to infer dark matter halo masses (Zwicky 1937; Huchra & Geller 1982; Moore, Frenk & White 1993; Carlberg et al. 1996; Eke et al. 2004; Berlind et al. 2006).

The target selection algorithm and area covered by a redshift survey relate to the redshift range and volume surveyed. The industry of these surveys started in the 1980s with surveys of ∼2500 galaxies over large sky areas (Davis et al. 1982; Saunders et al. 1990) and a deeper survey of 330 galaxies over 70 deg^2 (Peterson et al. 1986). It expanded and diversified in the 1990s with surveys such as the wide-but-shallow CfA2 redshift survey, Las Campanas Redshift Survey, ESO Slice Project and the deep-but-narrow Canada–France Redshift Survey. Fig. 1 shows the surface density of galaxy spectra versus area for these and other surveys, and Table 1 gives selections and references. The target density is a wavelength-independent metric for depth, at least for high-completeness magnitude-limited surveys. The advent of multi-object spectrographs such as the Two-Degree Field (2dF; Lewis et al. 2002) and Sloan Digital Sky Survey (SDSS; York et al. 2000) telescope have enabled redshift surveys of $>10^5$ galaxies: the 2dF Galaxy Redshift Survey (2dFGRS) and SDSS Main Galaxy Sample (MGS).

The Galaxy And Mass Assembly (GAMA) project has at its core a galaxy redshift survey using the upgraded 2dF instrument AAOmega on the Anglo-Australian Telescope (AAT). GAMA will eventually incorporate a range of new surveys from ultraviolet (UV), visible, infrared (IR) and radio wavelengths (Driver et al. 2009). The redshift survey uses for its input catalogue data from the SDSS and United Kingdom InfraRed Telescope (UKIRT). The primary goals of the redshift survey are measurement of the halo mass function (Eke et al. 2006), galaxy stellar mass function (Cole et al. 2001) and the merger rates of galaxies (De Propris et al. 2005): for systems of the lowest possible masses (at low redshift $z < 0.05$), and for their evolution out to $z \sim 0.5$. In terms of depth and area of magnitude-limited surveys (squares in Fig. 1), GAMA bridges the gap between the wide but shallower surveys like 2dFGRS and SDSS MGS, and the deep but narrower surveys such as those using the VIsible MultiObject Spectrograph (VIMOS) on the Very Large Telescope (VLT).

The outline of the paper is as follows. The imaging data, magnitude measurements and initial catalogues are described in Section 2. The target selection is described in Section 3: star–galaxy separation, magnitude limits and other quality checks. The pre-existing and GAMA spectroscopic data sets are outlined in Section 4. An analysis of results as pertaining to the star–galaxy separation and other selection criteria is presented in Section 5. In other survey papers, the scientific and multiwavelength data base aims are described in Driver et al. (2009), and the tiling strategy is described in Robotham et al. (2009).

Magnitudes are corrected for Milky Way extinction using the dust maps of Schlegel, Finkbeiner & Davis (1998) except for fibre magnitudes. Extinction in the bands u, g, i, z, J, K are obtained from SDSS r-band extinction using fixed ratios (1.873 864, 1.378 771, 0.758 270, 0.537 623, 0.323, 0.131).[1] The UKIRT magnitudes are converted to the AB system using $J_{\rm AB} = J + 0.94$ and $K_{\rm AB} = K + 1.90$ (Hewett et al. 2006). The contours used to represent bivariate distributions (Figs 6–7, 10–13, 15) are logarithmically spaced in number density, with four levels per factor of 10.

2 IMAGING

2.1 Sloan Digital Sky Survey and GAMA regions

The SDSS project (York et al. 2000; Stoughton et al. 2002) has used a dedicated 2.5-m telescope to image ∼10^4 deg^2 and to obtain spectra of ∼10^6 objects (Adelman-McCarthy et al. 2008). The imaging was obtained through five broad-band filters, *ugriz* with effective wavelengths of 355, 470, 620, 750 and 895 nm, using a mosaic CCD camera consisting of five rows and six columns (Gunn et al. 1998). Observations with a 0.5-m photometric telescope (Hogg et al. 2001) are used to calibrate the 2.5-m telescope images using the $u'g'r'i'z'$ standard star system (Fukugita et al. 1996; Smith et al. 2002). The GAMA survey targets were selected using DR6 imaging.[2]

The imaging was obtained by drift scanning along a strip defined in an SDSS coordinate system. Two strips, designated N and S, are interleaved to fill in the gaps between the camera columns and are combined to make one stripe. The choice for the GAMA survey consisted of the southern-most stripes (Dec. $< 3^\circ$) for good access from Southern observatories. The contiguous SDSS coverage of Stripes 9–12 was chosen to allow GAMA regions that are 4° wide: an estimated requirement for group finding and measurement of the

[1] The SDSS extinction ratios are given in table 22 of Stoughton et al. (2002). The ratios for J- and K-band extinctions were obtained from UKIRT Wide-Field Camera (WFCAM) science archive (Hambly et al. 2008) data matched to SDSS r-band extinction.

[2] We are aware that a new photometric calibration was implemented for the DR7 release (Padmanabhan et al. 2008; Abazajian et al. 2009). However, the magnitude changes are typically less than 0.02 mag and therefore, for consistency, we have not used the DR7 magnitudes because we started spectroscopic observations prior to this release.

Table 1. List of field galaxy redshift surveys. The surveys shown in Fig. 1 are listed in order of increasing area. They are mostly magnitude-limited galaxy samples except for some with colour selection (CS). The information was obtained from the references and the survey web sites.

Abbreviation	Survey name	Selection(s)	Area/deg ^{2}	Reference
CFRS	Canada–France Redshift Survey	$I_{AB} < 22.5$	0.14	Lilly et al. 1995
LBG-z3	Lyman Break Galaxies at $z \sim 3$ Survey	$R_{AB} < 25.5$ with CS[a]	0.38	Steidel et al. 2003
VVDS-deep	VIMOS VLT Deep Survey deep sample	$I_{AB} < 24.0$	0.5	Le Fèvre et al. 2005
CNOC2	Canadian Network for Obs. Cosmology 2 . . .	$R < 21.5$	1.5	Yee et al. 2000
zCOSMOS	Redshifts for the Cosmic Evolution Survey	$I_{AB} < 22.5, I_{AB} \lesssim 24$ with CS[b]	1.7	Lilly et al. 2007
DEEP2	Deep Evolutionary Exploratory Probe 2 . . .	$R_{AB} < 24.1$ with CS[c]	2.8	Davis et al. 2003
Autofib	Autofib Redshift Survey	$b_J < 22.0$	5.5	Ellis et al. 1996
H-AAO	Hawaii+AAO K-band Redshift Survey	$K < 15.0$	8.2	Huang et al. 2003
AGES	AGN and Galaxy Evolution Survey	incl. $R < 20.0, B_W < 20.5$	9.3	Watson et al. 2009
VVDS-wide	VIMOS VLT Deep Survey wide sample	$I_{AB} < 22.5$	12.0	Garilli et al. 2008
ESP	ESO Slice Project	$b_J < 19.4$	23.3	Vettolani et al. 1997
MGC	Millennium Galaxy Catalogue	$B < 20.0$	37.5	Liske et al. 2003
GAMA	Galaxy And Mass Assembly Survey	$r < 19.8, z < 18.2, K_{AB} < 17.6$	144	This paper
2SLAQ-lrg	2SLAQ Luminous Red Galaxy Survey	$i < 19.8$ with CS[d]	180	Cannon et al. 2006
SDSS-s82	SDSS Stripe 82 surveys	incl. $u \lesssim 20, r < 19.5$ with CS[e]	275	Adelman-McCarthy et al. 2006
LCRS	Las Campanas Redshift Survey	$R < 17.5$	700	Shectman et al. 1996
WiggleZ	WiggleZ Dark Energy Survey	NUV < 22.8 with CS[f]	1 000	Drinkwater et al. 2010
2dFGRS	2dF Galaxy Redshift Survey	$b_J < 19.4$	1 500	Colless et al. 2001
DURS	Durham-UKST Redshift Survey	$b_J < 17.0$	1 500	Ratcliffe et al. 1996
SAPM	Stromlo-APM Redshift Survey	$b_J < 17.1$ (1 in 20 sampling)	4 300	Loveday et al. 1992
SSRS2	Southern Sky Redshift Survey 2	$B < 15.5$	5 500	da Costa et al. 1998
SDSS-mgs	SDSS Main Galaxy Sample	$r < 17.8$	8 000	Strauss et al. 2002
SDSS-lrg	SDSS Luminous Red Galaxy Survey	$r < 19.5$ with CS[g]	8 000	Eisenstein et al. 2001
6dFGS	6dF Galaxy Survey	$K < 12.7, b_J, r_F, J, H$ limits	17 000	Jones et al. 2009
CfA2	Center for Astrophysics 2 Redshift Survey	$B < 15.5$	17 000	Falco et al. 1999[h]
PSCz	*IRAS* Point Source Catalog Redshift Survey	60 μm $_{AB} < 9.5$	34 000	Saunders et al. 2000
2MRS	2MASS Redshift Survey	$K < 12.2$	37 000	Erdoğdu et al. 2006

Notes. [a]CS by U-band 'dropouts' for photometric redshifts (z_{ph}) $\sim$ 2.5–3.5; [b]CS for $z_{ph} \sim$ 1.4–3.0, deeper limit over 1 deg^2; [c]CS for $z_{ph} \gtrsim 0.7$; [d]CS for $z_{ph} \sim$ 0.45–0.8; [e]CS for $z_{ph} \lesssim 0.15$; [f]CS by FUV–NUV > 1.5 (GALEX bands) and $20.5 < r < 22.5$ for $z_{ph} \sim$ 0.5–1.0; [g]CS for $z_{ph} \sim$ 0.2–0.5; [h]reference is for the updated Zwicky catalog that includes CfA2 redshifts.

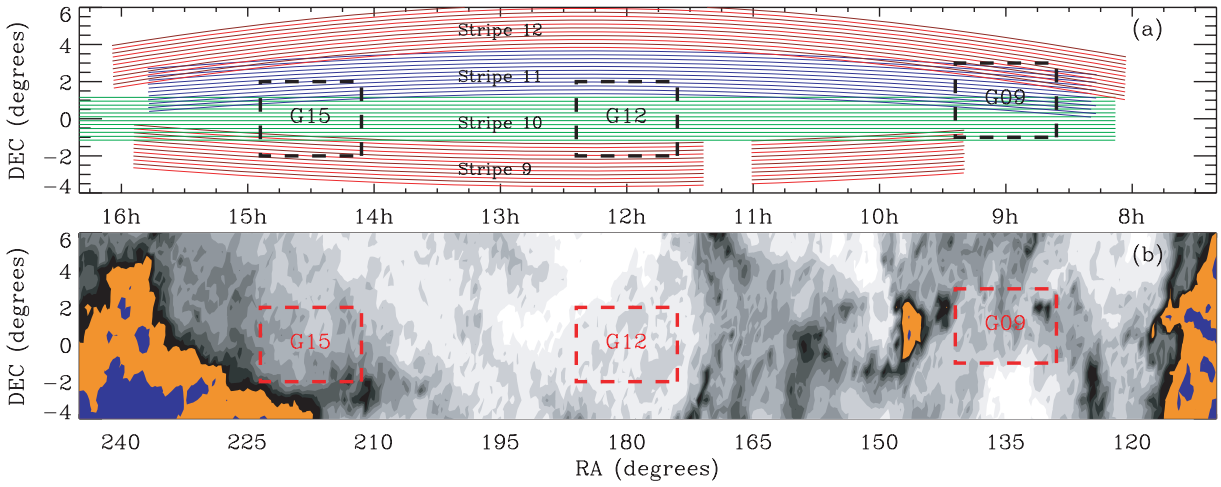

Figure 2. (a) Scan-line positions for SDSS Stripes 9–12. The GAMA regions are outlined using dashed lines. The 12 scan-lines for each stripe are the result of interleaving north and south strips each with six camera columns. (b) GAMA regions in relation to the dust map of Schlegel et al. (1998). The colours represent SDSS r-band extinction in magnitude ranges: <0.06 white; 0.06–0.20 grey-scale; 0.20–0.25 black; 0.25–0.5 orange and >0.5 blue.

halo mass function at $z < 0.1$ (Driver et al. 2009). Fig. 2 shows these regions in relation to the SDSS stripes and Milky Way extinction. They each cover $4^\circ \times 12^\circ$ and are centred on 9, 12 and 14.5 h. The RA and Dec. ranges are given in Table 2.

The SDSS produces various magnitude measurements (Stoughton et al. 2002). These include the following.

(i) Petrosian magnitudes measured using a circular aperture that is twice the Petrosian radius. The radius is determined using the surface brightness profile of the object in the r band.

(ii) Model magnitudes determined from the best fit of an exponential or de Vaucouleurs profile. The shape parameters (major–minor axes ratio, position angle, scale radius) are determined from

Table 2. The GAMA regions defined in J2000 coordinates.

G09	$129^{\circ}.0 < \mathrm{RA} < 141^{\circ}.0$	$-1^{\circ}.0 < \mathrm{Dec.} < 3^{\circ}.0$
G12	$174^{\circ}.0 < \mathrm{RA} < 186^{\circ}.0$	$-2^{\circ}.0 < \mathrm{Dec.} < 2^{\circ}.0$
G15	$211^{\circ}.5 < \mathrm{RA} < 223^{\circ}.5$	$-2^{\circ}.0 < \mathrm{Dec.} < 2^{\circ}.0$

the *r*-band image, while only the amplitude is fitted in the other bands.

(iii) Point spread function (PSF) magnitudes determined from a fit using the PSF in each band.

(iv) Fibre magnitudes measured using a circular aperture that is 3 arcsec in diameter. For these magnitudes, no attempt is made to deblend overlapping objects. Their purpose is to provide an estimate of signal in the spectrographs.

These magnitude types are all used in our selection for various reasons. Note that we make no adjustment from the SDSS 3-arcsec fibre magnitudes to AAOmega 2-arcsec apertures. An average correction is 0.35 mag, with the 95 per cent range being from 0.15 to 0.6 mag (for galaxies with $18 < r < 20$).

The SDSS pipeline PHOTO also gives a number of flags for each measured source (table 9 of Stoughton et al. 2002). The most important for target selection is SATUR, which is set if any pixel in a source or its 'parent' is saturated. This can be used to effectively exclude deblends of bright stars. We also consider the PARENTID of sources, which can be used to group together objects that may be significantly overlapping. This is used in the visual classification process (Section 3.5) to identify deblended parts of galaxies.

The initial input catalogue was selected from the DR6.PHOTOOBJ table with, in addition to magnitude limits and area restrictions, the following criteria (in SQL):

```
(mode = 1) or
(mode = 2 and ra < 139.939 and dec < -0.5 and
(status & dbo.fphotostatus('OK_SCANLINE')) > 0)
```

The MODE column is set to 1 for primary objects and to 2 for secondary objects, which are in areas where stripes and/or scan-lines overlap. However, Stripe 9 is mostly incomplete for G09 and thus secondary objects need to be selected from some Stripe 10 scan-lines in this region because the code assumes Stripe 9 is complete when determining the MODE values (see Fig. 2a, consider the extension of Stripe 9 to 8 h). The RA and Dec. limits above select the appropriate part of Stripe 10, and the OK_SCANLINE flag ensures that selected objects are not in the overlap edge areas of the scan-lines.

While data from Stripes 9–12 were used for GAMA target selection, data from Stripe 82 were used for early testing of our star–galaxy separation method. This was because of the available UKIRT *J*- and *K*-band coverage at the time and because of significant additional SDSS redshifts beyond the main SDSS surveys. The additional targets included selections for both resolved and unresolved sources (Adelman-McCarthy et al. 2006).

2.2 UKIRT Infrared Deep Sky Survey

The UKIRT Infrared Deep Sky Survey (UKIDSS; Dye et al. 2006; Lawrence et al. 2007) is a project using the WFCAM (Casali et al. 2007) on the 3.8-m UKIRT. The WFCAM instrument consists of four 2k × 2k HgCdTe detectors in a two-by-two pattern. Each detector covers $13.7 \times 13.7\,\mathrm{arcmin}^2$ and is separated from neighbouring detectors by 12.9 arcmin (94 per cent of each detector's active length). Thus, four observations can be interleaved to form a contiguous $0.9^{\circ} \times 0.9^{\circ}$ tile. The available filters are *ZYJHK* with effective wavelengths of 0.88, 1.03, 1.25, 1.63 and 2.20 μm (Hewett et al. 2006). The UKIDSS consists of a number of different subsurveys, including the Large Area Survey (LAS) obtaining imaging in *YJHK* over $>2000\,\mathrm{deg}^2$ within the SDSS main survey regions.

There is a dedicated pipeline for reducing and a system for archiving the UKIDSS data (Hambly et al. 2008). However, we did not use the fully reduced data product catalogues for the GAMA regions when we incorporated UKIDSS LAS data into our selection criteria. This was partly because of known problems with the deblending algorithm, and also our desire to have control over aperture matched photometry. Reduced LAS images, the detector frames, were obtained from the archive. These were scaled to a common background and gain, and *YJHK* mosaics were produced using the AstrOmatic SWarp program (Bertin et al. 2002). A systematic study of the calibration errors in Hodgkin et al. (2009) finds that the photometry is accurate to better than 0.02 mag rms when tested against the Two Micron All Sky Survey (2MASS; Skrutskie et al. 2006) for *J*, *H* and *K* bands, making a global recalibration unnecessary.

Each GAMA region has pixel aligned 20 GB mosaics for each band, alleviating problems due to multiple edge extractions and allowing us to use matched aperture photometry. The final mosaics have a $0.4\,\mathrm{arcsec\,pixel}^{-1}$ scale, use median co-addition in overlap regions and interpolate the resampled pixels using Lanczos resampling level 3. These latter setting is as suggested in the SWarp manual. The use of matched aperture photometry is important for improving the quality of the galaxy colours, and our star–galaxy separation. SExtractor (Bertin & Arnouts 1996) was run in dual mode on the *J* and *K* images, with the source positions and sizes defined in the *K* band, using default parameters. This catalogue was then matched to an initial SDSS catalogue (for GAMA) within a 2 arcsec tolerance using STILTS (Taylor 2005), with the nearest match chosen when there were multiple matches. Fig. 3 shows the *J*- and *K*-band LAS coverage used for target selection prior to AAT observations in 2009. While the UKIDSS coverage will be completed and may be used for future targeting, any analysis considering completeness as a function of position will need to take account of the UKIDSS coverage prior to the 2009 observations.

The output from SExtractor gives a number of flux measurements. Here we generally use the standard AUTO magnitude, based on an elliptical aperture defined using Kron's (1980) algorithm. These AUTO magnitudes are used for *K*-band selection and for $J - K$ colours as part of the star–galaxy separation criteria. For early tests of our star–galaxy separation using Stripe 82 data (Section 3.1), we used the available UKIDSS pipeline APERMAG3 measurements, which are determined using 2.0 arcsec circular apertures.

The fidelity of additional UKIDSS targets is a key concern. The imaging used in this work has already passed the basic quality assessments discussed in Dye et al. (2006) and Warren et al. (2007). This involves removing completely corrupted data and images affected by moon ghosting and other serious visual artefacts. To further ensure the quality of additional near-IR selected objects, two precautions were taken. First all targets had to possess an SDSS counterpart (see above), and secondly selected UKIDSS targets were visually inspected by a small group within the GAMA team (Section 3.5). This level of care goes a great way to mitigating against any data quality issues in the original UKIDSS data. The fraction of fibres placed on spurious artefacts should be small since they would have to be present in SDSS and UKIDSS imaging at the same position in the sky.

Fig. 4 shows the *K*-band galaxy counts using the derived AUTO magnitudes in the GAMA regions both from a match to an SDSS $r < 22$ catalogue and from a match to an $r < 20.5$ catalogue. There

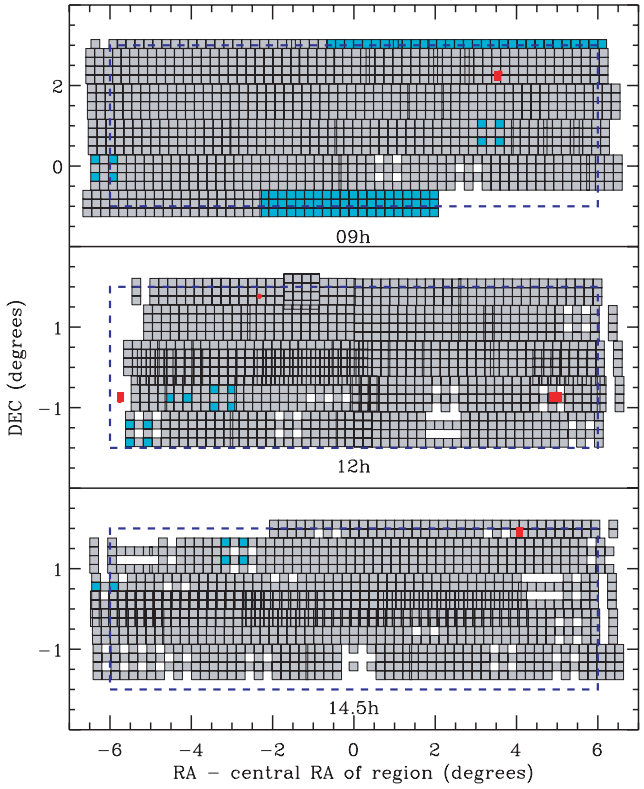

Figure 3. UKIDSS *J*- and *K*-band coverage for AAT observations in 2009. The squares represent the WFCAM frames: filled grey if *J* and *K* bands were available, and cyan if only the *K* band was available. The *K*-band areal coverage of G09, G12 and G15 is 96.5, 93.5 and 88.2 per cent, respectively. The red areas show the largest areas missing from the SDSS coverage because of masking around the brightest stars ($3.5 < V < 4.5$; HR 3665, HR 4471, HR 4540, HR 4689, HR 5511) and related 'timed out' frames.

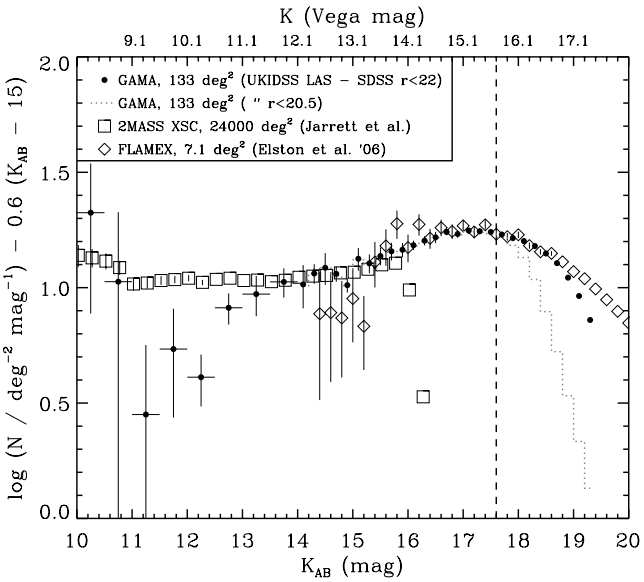

Figure 4. *K*-band galaxy counts for the UKIDSS GAMA regions, 2MASS Extended Source Catalog and FLAMINGOS Extragalactic Survey. The *y*-axis shows the logarithmic counts with the slope for a non-evolving Euclidean universe subtracted. The dotted line shows the drop in counts at the faint end when the SDSS match is restricted to $r_{\rm model} < 20.5$. The vertical dashed line is the limit used for the *K*-band selection (Section 3.2). The GAMA errors were determined from standard errors using six different areas (two per GAMA region); while the errors for the other surveys were obtained from tables provided by T. Jarrett and A. Gonzalez, respectively.

is excellent agreement between the UKIDSS LAS and 2MASS counts (Jarrett et al. 2000, 2010) from about 12.5 to 15.8 AB mag. At brighter magnitudes, the discrepancy is not of concern for targeting because these bright galaxies will have redshifts anyway; the discrepancy could be caused by cosmic variance and/or the use of the 2 arcsec tolerance. At fainter magnitudes, the 2MASS incompleteness is evident, while the UKIDSS counts are in good agreement with the FLAMINGOS Extragalactic Survey (FLAMEX; Elston et al. 2006) counts to $K_{\rm AB} \lesssim 18.8$. The agreement in the galaxy counts between these surveys demonstrates consistency in the derived magnitudes and star–galaxy separation, which for GAMA is described in the following section.

3 TARGET SELECTION

3.1 Star–galaxy separation

Automatic separation of stars and galaxies from images has typically been done using shape or intensity profile measurements (e.g. MacGillivray et al. 1976; Maddox et al. 1990). The SDSS star–galaxy separation parameter (Strauss et al. 2002) is defined as

$$\Delta_{\rm sg} = r_{\rm psf} - r_{\rm model}, \quad (1)$$

where $r_{\rm psf}$ and $r_{\rm model}$ are the *r*-band PSF and model magnitudes. The value deviates from zero when the de Vaucouleurs or exponential profile fit accounts for more flux than only using a PSF fit, i.e. a significant deviation from zero indicates that the intensity profile

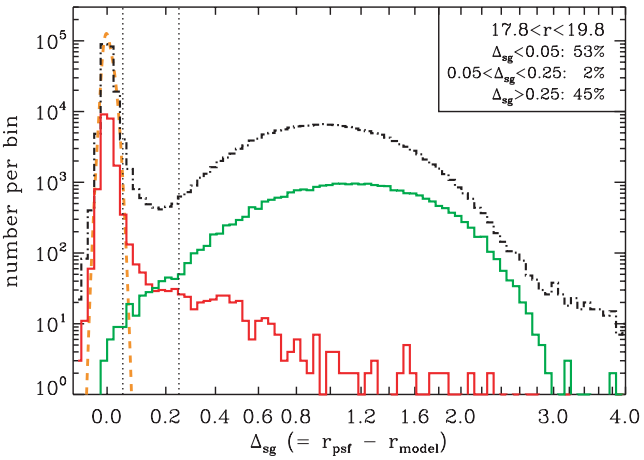

Figure 5. Histogram of $\Delta_{\rm sg}$ for Stripe 82 data. The *x*-axis stretch is linear in $\ln(1 + \Delta_{\rm sg})$ (bin size is 0.02). The dash–dotted histogram represents all objects, while the red histogram represents objects with confirmed stellar redshifts ($-0.002 < z < 0.002$), and the green histogram represents extragalactic sources with $0.002 < z < 0.35$. Note the *y*-axis is on a logarithmic scale and the orange dashed curve shows a double Gaussian fit to the stellar peak (FWHM ~ 0.025). The vertical dotted lines show the range for marginally resolved sources ($0.05 < \Delta_{\rm sg} < 0.25$).

is not well matched to the PSF. Fig. 5 shows a histogram in this parameter for objects with $17.8 < r_{\rm petro} < 19.8$ that are not deblended from a saturated object. Also shown are objects with confirmed stellar redshifts and galaxies with $0.002 < z < 0.35$ (from Stripe 82). The cut $\Delta_{\rm sg} > 0.24$ was the constraint used for star–galaxy

separation in the SDSS MGS.[3] With this selection, some galaxies that are compact will be missed, particularly as we target fainter than $r = 17.8$.

Our first cut is to select objects with $\Delta_{sg} > 0.05$ (nominally marginally or well resolved). This removes the Gaussian core of objects that are unresolved, which are almost all stars and quasars. However, this cut is still too inclusive of stars for targeting efficiency, so further cuts need to be applied. In particular, the $0.05 < \Delta_{sg} < 0.25$ region probably includes many double-star systems as well as marginally resolved galaxies. The latter are selected using colour cuts based on our UKIDSS–SDSS-matched catalogue.[4]

A UKIDSS–SDSS star–galaxy separation was determined using data from Stripe 82. Fig. 6(a) shows a plot of $(J - K)_{apermag3}$ versus $(g - i)_{model}$ for objects with $\Delta_{sg} < 1.0$ and $17.8 < r_{petro} < 19.8$ (i.e. fainter than SDSS MGS within GAMA selection). A colour–colour diagram using these bands was utilized by Ivezić et al. (2002) to assess the success of SDSS star–galaxy separation and similarly by Elston et al. (2006), with $B_W - I$ instead of $g - i$, for the FLAMEX star–galaxy separation.

From selected sources, we fit the stellar locus with a quadratic. A new star–galaxy separation parameter is defined as the $J - K$ separation from the locus, which is shown by the blue dashed line. The parameter is given by

$$\Delta_{sg,jk} = J_{AB} - K_{AB} - f_{locus}(g - i), \quad (2)$$

where

$$f_{locus}(x) = \begin{cases} -0.7172 & x < 0.3, \\ -0.89 + 0.615x - 0.13x^2 & \text{for } 0.3 < x < 2.3, \\ -0.1632 & x > 2.3. \end{cases} \quad (3)$$

Fig. 6(b) shows $\Delta_{sg,jk}$ versus $(g - i)_{model}$, with symbols representing samples that have measured redshifts. The cut $\Delta_{sg,jk} > 0.20$ is used to select extragalactic sources among the objects with $0.05 < \Delta_{sg} < 0.25$ (the success and completeness of this UKIDSS–SDSS star–galaxy separation are presented later in Section 5.1).

Not all objects have measured $J - K$. For these objects we lower the Δ_{sg} cut for fainter objects to $\Delta_{sg} > f_{sg,slope}(r_{model})$, where

$$f_{sg,slope}(x) = \begin{cases} 0.25 & x < 19.0, \\ 0.25 - \frac{1}{15}(x - 19) & \text{for } 19.0 < x < 20.5, \\ 0.15 & x > 20.5. \end{cases} \quad (4)$$

Fig. 7 shows the distribution in Δ_{sg} versus r_{model}, with the cut shown by the red dashed line. This is appropriate because the sky density of objects that are galaxies compared to double stars, in the marginally resolved region, is increasing towards fainter magnitude limits.

[3] $\Delta_{sg} > 0.3$ is the MGS criteria quoted in Strauss et al. (2002) but the limit was later reduced to 0.24 following the change in the model magnitude code at DR2 (Abazajian et al. 2004).

[4] Note that even with UKIDSS–SDSS colour selection, selecting objects with $\Delta_{sg} < 0.05$ would result in a large stellar contamination to our galaxy sample. The median PSF full width at half-maximum for the SDSS r band is 1.4 arcsec in the GAMA regions, with 95 per cent of 'fields' having seeing better than 2.1 arcsec. While the UKIDSS LAS K-band seeing is typically better than ∼1 arcsec, we have not yet modelled the PSF variation accurately and thus prefer to use the well-established SDSS profile separator rather than one based on UKIDSS (which in any case does not cover all the GAMA area). Our UKIDSS–SDSS colour selection will mitigate against variation in the reliability of the SDSS profile separation.

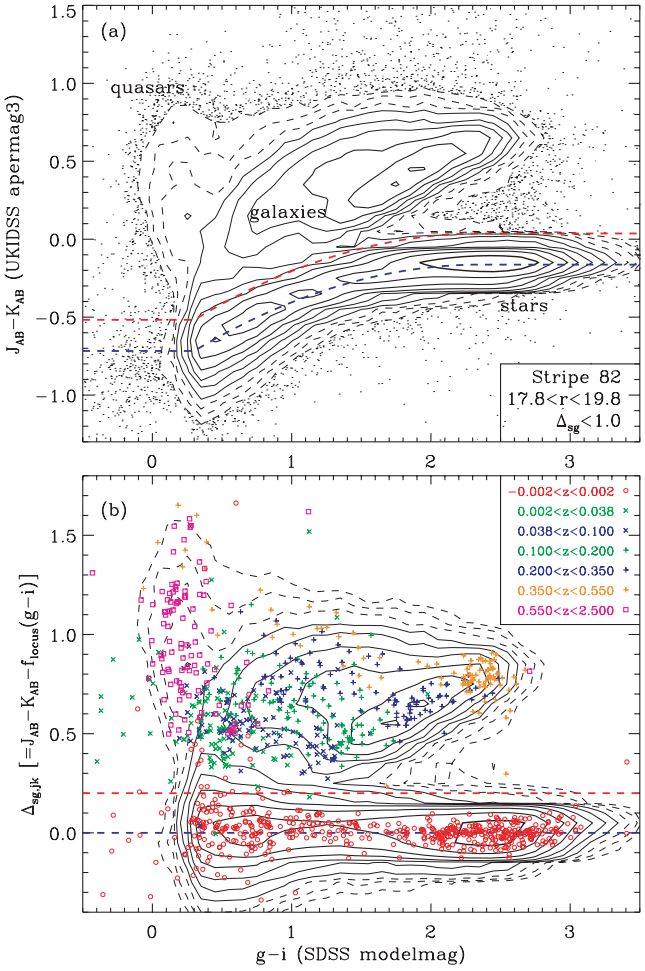

Figure 6. (a) Star–galaxy separation in colour–colour space. The blue dashed line represents a fit to the stellar locus over the range $0.3 < g - i < 2.3$ and constant $J - K$ either side of the fitted range (equation 3); while the red dashed line is $+0.2$ in $J - K$ from this fit. (b) $J - K$ star–galaxy separation parameter versus $g - i$ for populations over different redshift ranges. From objects with measured redshifts in Stripe 82, 500 stars and 100 in each extragalactic redshift range were selected at random. The red line shows the $\Delta_{sg,jk}$ cut.

In summary, the overall star–galaxy separation is given by

$$\Delta_{sg} > 0.25$$

or

$$\Delta_{sg} > 0.05 \text{ and } \Delta_{sg,jk} > 0.20$$

or

$$\Delta_{sg} > f_{sg,slope}(r_{model}) \text{ and no } J - K \text{ measurement.} \quad (5)$$

Only objects satisfying these criteria are targeted in the main survey.

The GAMA UKIDSS selection was based on non-pipeline SExtractor magnitudes. Thus, the final star–galaxy separation (equation 2) was determined using auto mags for $J - K$ and SDSS model mags for $g - i$ (data from Stripes 9–12). Fig. 8 shows histograms in $\Delta_{sg,jk}$ using these magnitudes. In order to test the position of the stellar locus, unresolved samples ($\Delta_{sg} < 0.05$; not used for targeting) were selected in separate $1^\circ \times 1^\circ$ regions (grey lines in Fig. 8). The median value of $\Delta_{sg,jk}$ within each region varied from -0.05 to 0.04 with 90 per cent of the region values between

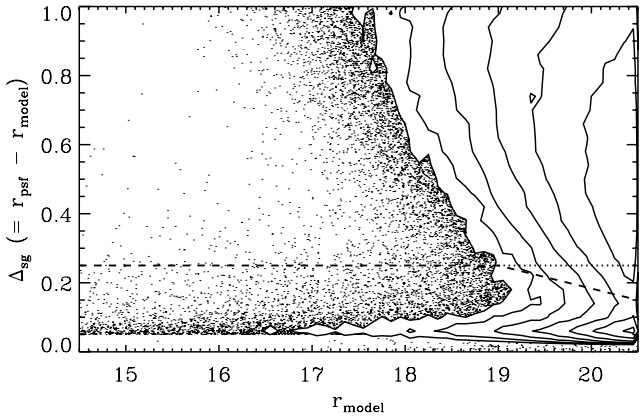

Figure 7. Star–galaxy separation regions. Above $\Delta_{sg} = 0.25$, objects are selected as a spectroscopic target regardless of $J - K$ colour (as per AAT observations in 2008 and SDSS MGS). Below the dashed line, objects are selected if they satisfy the $J - K$ star–galaxy separation criteria ($\Delta_{sg,jk} > 0.2$). While above the dashed line but with $\Delta_{sg} < 0.25$ (triangular region at $r > 19$), objects are selected if $\Delta_{sg,jk} > 0.2$ or there is no $J - K$ measurement.

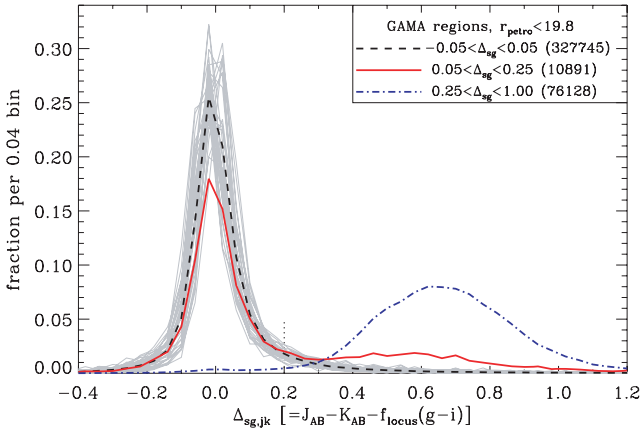

Figure 8. Histograms in $J - K$ star–galaxy separation parameter using SExtractor AUTO magnitudes. The histograms represent UKIDSS–SDSS matched samples divided into unresolved (not selected for targeting), marginally resolved (selected if $\Delta_{sg,jk} > 0.2$) and strongly resolved (selected regardless of $\Delta_{sg,jk}$) in SDSS r-band imaging. The thin grey line histograms represent unresolved samples in 36 randomly selected $1^\circ \times 1^\circ$ regions.

−0.03 and 0.02. This demonstrates that the stellar locus fit applies to AUTO mags equally well.

3.2 Magnitude limits

The main scientific goal of GAMA that drives the choice of the minimum width of the survey geometry, and the magnitude selection, is the measurement of the halo mass function (Driver et al. 2009). We chose r-band selection because it is most directly correlated with spectral signal-to-noise ratio (S/N) obtained (the filter falls in the middle range of the spectrograph). This ensures a high redshift success rate for a given target density. The r-band limits were chosen to give an average target density up to an order of magnitude higher than the SDSS MGS (90 deg^{-2}) and 2dFGRS (140 deg^{-2}). Given the limitations of efficient observing over two or three lunations each year, three fields were chosen covering 6 h in RA. We compromised between area and depth by choosing a limit of $r < 19.4$ in G09 and G15 (670 deg^{-2}), and $r < 19.8$ in G12 (1070 deg^{-2}). These

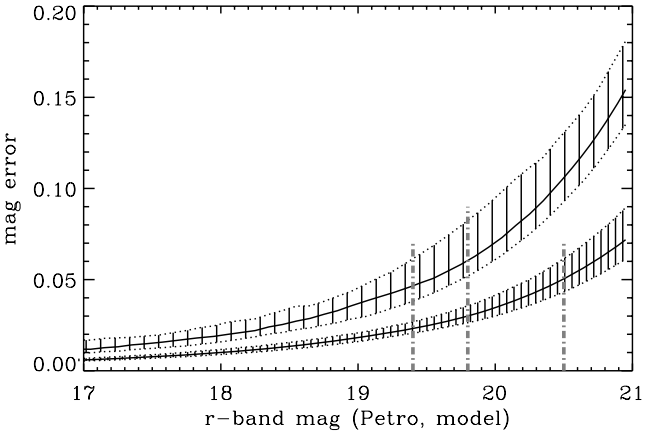

Figure 9. Magnitude errors versus magnitude. The solid lines show the median errors obtained from the SDSS catalogue, with the regions representing the interquartile range (top for Petrosian, lower for model magnitudes). The vertical dash–dotted lines represent the r-band limits used in this paper (19.4 and 19.8 using Petrosian, and 20.5 using model magnitudes).

were defined using Petrosian magnitudes, following the strategy of the SDSS MGS.

In consideration of measuring the stellar mass function, we included a near-IR selection using SDSS z band and UKIDSS K band. To ensure reliability and reasonable redshift success rate, these were also constrained by an r-band selection ($r_{model} < 20.5$). The choice of SDSS model magnitudes rather than Petrosian is a consequence of the noise statistics. For Petrosian magnitudes, the noise is well behaved to $r \simeq 20$ (Stoughton et al. 2002), while for fainter objects the model magnitudes are more reliable. Fig. 9 shows the pipeline-output magnitude errors versus magnitude. Also, the K-band selection was based on AUTO magnitudes, and both AUTO and model magnitudes use elliptical apertures. The additional selections were a small sample to $z_{model} < 18.2$ and a sample to $K_{AB,auto} < 17.6$.

Within the GAMA regions, the main survey selections are given by

$$
\begin{aligned}
&r_{petro} < 19.4 \\
&\text{or} \\
&r_{petro} < 19.8 \ \text{ and in the G12 area} \\
&\text{or} \\
&z_{model} < 18.2 \ \text{ and } \ r_{model} < 20.5 \\
&\text{or} \\
&K_{AB,auto} < 17.6 \ \text{ and } \ r_{model} < 20.5.
\end{aligned}
\tag{6}
$$

Including the near-IR selections increases the G12 target density marginally (to 1080 deg^{-2}) while increasing the G09 and G15 target density to 720 deg^{-2}. Fig. 10 shows the colour bias for the near-IR selections. The z-band selection is complete to $(r - z)_{model} < 2.3$ at the faint limit, while the K-band selection is complete to $r_{model} - K_{AB,auto} < 2.9$ at the faint limit. A $z_{model} < 18.2$ selection is formally missing 0.3 per cent of objects because of the r_{model} limit, while a $K_{AB,auto} < 17.6$ selection is formally missing about 1 per cent of objects. This is after applying star–galaxy separation. However, only very red objects are missed, which are more likely to be stars in spite of the star–galaxy separation or have incorrectly measured colours caused by mismatched apertures in the case of $r - K$ (the practical impact of these joint limits is discussed later in Section 5.4). See

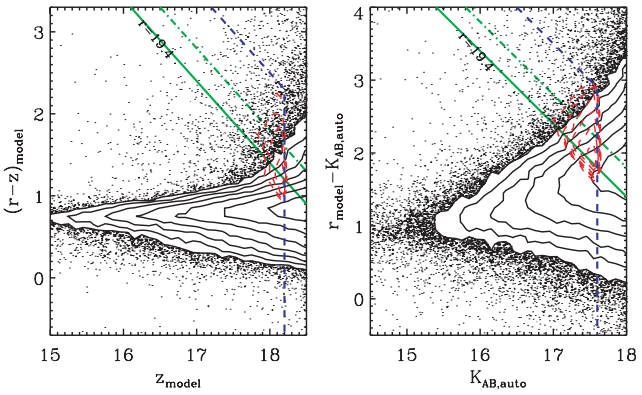

Figure 10. Colour versus magnitude distribution for a near-IR sample. The black contours and points represent potential galaxy targets. The blue dashed lines show the limits imposed by our selection including the constraint $r_{\rm model} < 20.5$. The green lines show $r = 19.4$ and 19.8 limits. The red contours represent most of the additional targets not selected by the $r_{\rm petro}$ limits. These contours extend below the solid green line because of differences between Petrosian and model magnitudes.

also Fig. 4: the $r < 20.5$ limit only makes an obvious impact in the galaxy number counts at $K_{\rm AB,auto} > 17.8$, which is above our selection limit.

3.3 Masking

In order to avoid targeting galaxies with bad photometry because they are near bright stars or satellite trails, an explicit mask was constructed. The bright-stars mask was based on stars down to $V < 12$ in the Tycho 2, Tycho 1 and *Hipparcos* catalogues. For each star, a scattered-light radius ($\mathcal{R}_{\rm s}$) was estimated based on the circular region over which the star flux per pixel is greater than five times the sky noise level. For each potential target, a mask parameter was defined as follows:

$$\begin{aligned} &\text{MASK\_IC\_12} = 1 && d \le \mathcal{R}_{\rm s}, \\ &\text{MASK\_IC\_12} = \mathcal{R}_{\rm s}/d \quad \text{for} && \mathcal{R}_{\rm s} < d \le 5\mathcal{R}_{\rm s}, \\ &\text{MASK\_IC\_12} = 0 && d > 5\mathcal{R}_{\rm s}, \end{aligned} \tag{7}$$

where d is the distance to a $V < 12$ star with radius $\mathcal{R}_{\rm s}$. In other words, the MASK_IC_12 value decreases from unity when $d \le \mathcal{R}_{\rm s}$ to 0.2 when $d = 5\mathcal{R}_{\rm s}$. A similar mask parameter MASK_IC_10 was defined using only $V < 10$ stars. In addition, objects within an SDSS data base mask for holes, satellite trails and bleeding pixels had these mask values set to unity. After testing, we chose to select only objects with MASK_IC_10 < 0.5 and MASK_IC_12 < 0.8.

The largest masked areas are shown in Fig. 3. These are between 0.01 and 0.07 deg^2 each. Most of the separate masked areas are significantly smaller (<0.001 deg^2 or <1 arcmin in radius). Overall, the total masked area is about 1.0 deg^2 and the unmasked area of the survey is estimated to be 143.0 deg^2.

The mask was insufficient to remove all or nearly all objects with bad photometry. Therefore, as per SDSS selection, objects were selected to be NOT SATUR from the FLAGS column in the PHOTOOBJ table. This basically excludes deblends of bright stars but will also reject galaxies that are blended with saturated stars. These however are likely to have bad photometry and falsely bright magnitudes. The stars causing this saturation, not accounted for by the Tycho mask, are probably around $V \sim 13$.

The saturated-flag masking is not ideal. This is particularly the case for large nearby galaxies for which the angular size of the galaxy is a significant factor in determining the excluded sky area. In other words, the probability of a large galaxy having SATUR set depends primarily on its size rather than the area of the diffracted and scattered light around stars. To increase the completeness of the input catalogue for large galaxies, exceptions for the mask and not-saturated criteria were made for galaxies from the Uppsala General Catalog (UGC; Cotton, Condon & Arbizzani 1999) and Updated Zwicky Catalog (UZC; Falco et al. 1999). In addition, exceptions to the not-saturated criteria were made for a selection of visually inspected galaxies that have NOT SATUR_CENTER. There are only 86 objects with an exception flag set (selected as part of the visual classification process described in Section 3.5).

In summary, the criteria for including objects is given by

$$\begin{aligned} &(\text{MASK\_IC\_10} < 0.5 \text{ and } \text{MASK\_IC\_12} < 0.8 \text{ and} \\ &\text{not SATUR}) \\ &\text{or the exception flag is set.} \end{aligned} \tag{8}$$

3.4 Surface brightness limits

In addition to the implicit surface brightness (SB) limits from star–galaxy separation and detection, an explicit SB limit was applied, given by

$$15.0 < \mu_{r,50} < 26.0, \tag{9}$$

where $\mu_{r,50}$ is the effective SB in mag arcsec^{-2} within the 50 per cent light radius in the r band (equation 5 of Strauss et al. 2002). Anything of lower SB is very likely to be an artefact, and anything of higher SB is a star.

Fig. 11 shows the distribution of objects in $r_{\rm fibre}$ versus $\mu_{r,50}$ for GAMA main-survey targets. The lower limit of 15.0 does remove some objects, probably stars, not rejected by the masking or star–galaxy separation criteria (equation 5). The limit for $\mu_{r,50}$ of 26.0 is 1.5 mag deeper than the SDSS MGS cut, and is the point at which most of the objects are clearly artefacts. Note that the SDSS photometric pipeline is not complete for $\mu_{r,50} > 23$ (figs 2–3 of Blanton et al. 2005). Additional low-SB candidates could be recovered by searching coadded g, r and i images (Kniazev et al. 2004). Nevertheless, without deeper imaging, the data will remain incomplete at low SB well before our explicit limit.

In addition to the explicit SB limits given in equation (9), which we use to reject objects from our science catalogue, we include a restriction on the fibre magnitudes:

$$17.0 < r_{\rm fibre} < 22.5 \tag{10}$$

for targets allocated to the AAOmega observation schedule. This is a practical restriction, with a bright limit to avoid significant cross-talk in the spectrograph and a faint limit because the redshift success is very low. Selected fibre bright targets without a known redshift will be observed with a 2-m-class telescope, and, in principle, selected fibre faint targets will be observed with an 8-m-class telescope. At the bright end, a more restrictive cut on star–galaxy separation is also justified (see later in Section 5.2).

3.5 Visual classification

Sources with, for example, $\mu_{r,50} > 23$ have a high probability of being artefacts, deblends of stars or the outer parts of galaxies. One of us (JL) has written a code to facilitate the visual classification of such sources. A VIS_CLASS variable, initially with zero value, could be changed to the following for each source on inspection:

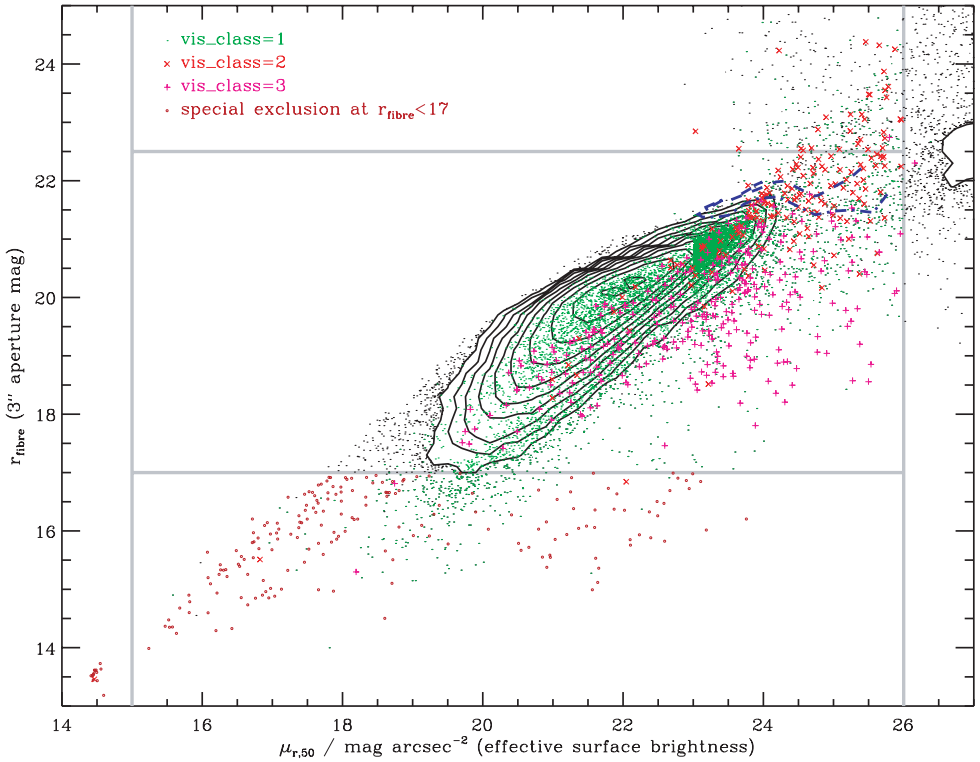

Figure 11. Bivariate distribution of $r_{\rm fibre}$ versus $\mu_{r,50}$. The black contours and points represent objects that are not masked and pass star–galaxy separation. The grey lines outline the selection limits: $15.0 < \mu_{r,50} < 26.0$ is the restriction for the science catalogue; while objects with fibre magnitudes fainter than 22.5 or brighter than 17.0 are not included in the AAOmega observation schedule. The green dots represent objects with VIS_CLASS = 1; the red crosses VIS_CLASS = 2, and the pink crosses VIS_CLASS = 3. The small red circles at $r_{\rm fibre} < 17$ are probably stars based on a stricter star–galaxy separation criteria (Section 5.2). The blue dash–dotted (dashed) line corresponds to 50 per cent (30 per cent) redshift success rate for objects on or near the line.

1. possibly a target,
2. not a target (no evidence of galaxy light),
3. not a target (not the main part of a galaxy).

First, sources with the following flags all equal to zero, EDGE, BLENDED, CHILD, MAYBE_CR, MAYBE_EGHOST, were assumed to be good, essentially isolated and not included in any testing (VIS_CLASS set to 255). About 50 per cent of targets satisfy these criteria. From the remaining objects, sources were selected for visual classification if any of the following conditions applied: $\mu_{r,50} > 23$, $r_{\rm fibre} > 21$, $r_{\rm fibre} < 17$, MASK_IC_12 > 0.2, $r_{\rm model} < 15.5$, $r_{\rm petro} < 15.5$, $r_{\rm fibre} < r_{\rm model}$, $r_{\rm fibre} < r_{\rm petro}$, near UGC galaxy, within 3 arcsec of another target, Petrosian radius >10 arcsec. These indicate that the object could be the result of deblending of a large galaxy, an artefact or a bright star, e.g. diffraction spikes. In addition to the above criteria, other objects were included in the above process. Objects with the same PARENTID as an already classified VIS_CLASS = 3 object were selected. (The above selection was not developed in one go and there have been several iterations.) Finally, objects, with the same PARENTID, that are the brightest and nearest to any object to be tested were included. Objects that could be part of the same galaxy were viewed together where possible. One had to be certain to classify objects as 3 only if the main part was identified as a target.

The above selection produced a sample of about 12 500 objects for visual classification, by six observers. Every selected object was classified by three different observers. Of the selected potential main-survey targets (Fig. 11), VIS_CLASS = 1 was set in 92 per cent of cases, VIS_CLASS = 2 in 5 per cent of cases, and VIS_CLASS = 3 in 3 per cent of cases, based on agreement between two or all three classifiers, 9 and 90 per cent of cases, respectively. Some of the ambiguous cases were double checked, and a single-observer classification was selected in 1 per cent of cases. Objects with values of 2 or 3 were removed from the schedule of AAT observations, i.e. targets must satisfy

$$\text{VIS\_CLASS} \neq 2 \text{ and } \text{VIS\_CLASS} \neq 3. \quad (11)$$

In addition, the VIS_CLASS = 3 objects can be used to improve the photometry of some large galaxies by co-adding in the flux of the galaxy parts (or the 'parent' photometry can be used).

3.6 Number of targets

The total number of objects that are within the GAMA regions (Section 2.1), main-survey magnitude limits (equation 6) and $\Delta_{\rm sg} > 0.05$ is 143 728. Applying the stricter star–galaxy separation (equation 5) reduces the sample to 132 073. Removing objects by masking (equation 8), the SB limits (equation 9) and visual checking (equation 11) reduces the sample to 120 038. Of these, 825 were not included in the AAOmega observation schedule because they do not satisfy the fibre magnitude limits (equation 10). A more restrictive star–galaxy separation can be applied for brighter targets (discussed later and given in equation 12) that reduces the sample to 119 852. This is considered to be the main-survey sample. Note that these numbers apply to AAT observations in 2009; the numbers may change slightly with addition of complete $J - K$ UKIDSS.

Separating the main survey into r, z and K limited samples, the numbers are 114 520, 61 418 and 57 657, respectively. For $r_{\rm petro}$

Table 3. Other spectroscopic data in the GAMA regions. Tables were obtained from the survey web sites or the VizieR service.

Survey	File/table	Reference	Number of redshifts[a]	Number of $Q \geq 3$	Number of main survey unique[b]
SDSS	DR7 SPECOBJALL	Abazajian et al. (2009)	27 514	26 687[c]	13 170
2dFGRS	VII/250/2dfgrs	Colless et al. (2003)	11 490	11 180	3840
MGCz	VII/240/mgczcat	Driver et al. (2005)	4 008	3 835	1883
2SLAQ-LRG	J/MNRAS/372/425/catalog	Cannon et al. (2006)	2 256	2 109	227
6dFGS	DR3 SPECTRA	Jones et al. (2009)	299	270	55
UZC	J/PASP/111/438/catalog	Falco et al. (1999)	255	209[d]	13
2QZ	VII/241/2qz	Croom et al. (2004b)	5 359	4 317[e]	224
2SLAQ-QSO	2slaq_qso_public.cat	Croom et al. (2009)	2 414	2 098[e]	34

[a]The number of redshifts quoted are all those in the GAMA regions including duplicates and non-GAMA targets.
[b]The number corresponds to unique main survey targets with a $Q \geq 3$ redshift from the survey (prior to GAMA). In the case of multiple matches within 1 arcsec, the highest Q value match is used (nearest in case of equal Q): Q is limited to $\leq$4 for all surveys except SDSS.
[c]SDSS quality is given by $Q = 1 +$ (ZCONF > 0.2) + (zwarning_okay AND ZCONF > 0.7) + (ZCONF > 0.9) + (ZCONF > 0.99) where each term in brackets takes the value of unity if the condition is true and zero otherwise, and zwarning_okay takes the value unity if the following warning flags EMAB_INC, AB_INC, 4000BREAK are all zero.
[d]UZC quality is given by: $Q = 3$ if UZC class is 0 or 1 (secure identification), and $Q = 2$ if UZC class is 2, 3 or 4 (some confusion regarding identification).
[e]2QZ and 2SLAQ-QSO quality is given by: $Q = 3$ if original quality code was 11 (good identification and redshift); $Q = 2$ if 22, 12 or 21 and $Q = 1$ if 33, 23 or 32.

selected samples to 19.0, 19.4 and 19.8, the sample sizes are 60 407, 96 386 and 150 810, respectively. The latter is the *r*-selected main survey plus F2 additional targets, which are described in the following subsection.

3.7 Additional targets

In order to assess the spectrophotometry of the AAOmega spectra, three or four stars, classified as REDDEN_STD or SPECTROPHOTO_STD by SDSS, were observed in each configuration. These also had a bright fibre magnitude limit of 17 as per the main-survey targets.

The aim is to obtain high completeness (99 per cent), at least in terms of spectra obtained and ideally in terms of confirmed redshifts, for the main survey. This is set to reduce systematic uncertainties in GAMA's position dependent science cases, and is possible because a given patch of sky is potentially observed by ∼5– 10 2dF tiles depending on the local density of targets (see Robotham et al. 2009 for a description of the tiling strategy). Given this requirement, targeting becomes increasingly inefficient as the survey progresses (fewer targets without a redshift per tile). Filler targets were introduced to provide useful redshifts outside the main survey, and thus, maximize fibre usage. These have no high-level requirement on completeness. The filler selections are given by (F1) objects with detection in the Faint Images of the Radio Sky at Twenty-cm (FIRST) survey and matched to SDSS with $i_{\rm model} < 20.5$ including unresolved sources; (F2) $19.4 < r_{\rm petro} < 19.8$ galaxy targets in G09 and G15, aiming for equal depth with G12 and (F3) $g_{\rm model} < 20.6$ or $r_{\rm model} < 19.8$ or $i_{\rm model} < 19.4$ in G12, investigating variation in magnitude type and wavelength on selection. In total, there are about 50 000 filler targets.

4 SPECTROSCOPY

4.1 Existing data sets

While the GAMA target density is significantly higher than SDSS or 2dFGRS, the redshifts obtained by these and other surveys provide a non-negligible starting baseline. We incorporate a number of different surveys into our catalogue, defining a redshift quality Q, where necessary, as per the Colless et al. (2001) scheme such that $Q = 1$ means very poor or no redshift, $Q = 2$ means a possible but doubtful redshift, $Q = 3$ means a probable redshift and $Q = 4$ or 5 means a reliable redshift. The surveys included are given in Table 3.

From the $Q \geq 3$ non-GAMA redshifts in the GAMA regions as outlined in the table, about 40 000 are unique (considering matches within 1 arcsec to be the same object). The number of main survey targets with one of these redshifts is 19 446, matching within 1 arcsec except for some large galaxies within 3 arcsec of a 6dFGS or UZC redshift. The non-GAMA redshifts without a match to a GAMA target are primarily of stars and quasars. Objects with $Q \geq 3$ redshifts are given a lower priority in the AAOmega observation schedule.

4.2 AAOmega observations in 2008 and 2009

GAMA observations with the multi-object spectrograph AAOmega on the AAT took place in 2008 (January 12, February 29 to March 15, March 30 to April 05) and 2009 (February 27 to March 05, March 27 to April 02, April 17 to April 23). The 2dF robotic fibre positioner (Lewis et al. 2002) feeds a bench-mounted dual-beam spectrograph (Sharp et al. 2006). Two plates are used: while one is being configured (fibres placed), the other plate is in the focal plane feeding light to the spectrograph. There are up to 392 science fibres available in a single configuration. Excluding broken fibres, 20–25 fibres used for sky subtraction and three or four spectroscopic standards (Section 3.7), we targeted between 320 and 350 GAMA targets per configuration. Total exposure times used were typically 1 h (3 × 20 min). We observed up to eight configurations in a single night for a total of 267 observations over the 2 yr (91 015 spectra). The spectral coverage was from 370 to 880 nm.

The priorities assigned to targets were different between the 2 yr. The tiling scheme is described in detail by Robotham et al. (2009). Here, we summarize the priorities. In 2008 the targets consisted only of the *r*-band selection with $\Delta_{\rm sg} > 0.25$ (there was insufficient UKIDSS coverage at the time), without an already known redshift (Section 4.1) except for some cross-check data. The priorities were from high-to-low: (i) $r < 19.0$; (ii) $19.0 < r < 19.8$ in G12 within $\pm 0.^{\circ}5$ of the celestial equator; (iii) $19.0 < r < 19.4$ in G09 and G15, and remaining $19.0 < r < 19.8$ in G12. In addition, clustered targets in any of these categories were given a higher priority. A clustered target was defined as one within 40 arcsec of another target, where 40 arcsec is approximately the closest two fibres can be placed.

Table 4. GAMA spectra from AAT observations in 2008 and 2009.

Description	Number
Total spectra obtained	91 015
Spectroscopic standards	1 059
Unique targets	87 753
Repeated targets	2 203
$Q \geq 3$ unique targets[a]	82 696
$r < 19.0$ and $\Delta_{sg} > 0.25$	40 103
Main survey r selected	38 994
Main survey z, K selected	1 847
F1: radio selected	105
F2: $19.4 < r < 19.8$ in G09 and G15	1 029
F3: filler selection in G12	68
Other[b]	550

[a]The unique targets with redshifts are identified in the rows below. The $r < 19.0$ selection corresponds to the higher priority targets in the first year of AAT observations. The numbers shown in each row below this row do not include contributions already accounted for. Below the main survey are the F1–F3 filler targets (Section 3.7).
[b]The 'other' objects are mostly objects whose UKIDSS photometry has undergone revision since the second year of AAT observations, and VIS_CLASS = 3 objects that were observed prior to implementation of the visual classification.

This was to maximize the chances of observing as many close pairs as possible over 3 yr of observations. In 2009, now including UKIDSS selection for the star–galaxy separation and magnitude limits, the priorities were (i) clustered unobserved main-survey targets; (ii) unobserved main survey or clustered failed main survey, where failed means that a GAMA spectrum has been obtained with $Q \leq 2$; (iii) failed main survey; (iv) from F1, F2, F3 filler targets, and $Q = 3$ spectra taken with the old 2dF spectrographs (e.g. 2dFGRS).

From the first 2 yr of observing, first-pass reductions with 2DFDR (Croom, Saunders & Heald 2004a) and RUNZ (Saunders, Cannon & Sutherland 2004) have resulted in a 94 per cent redshift success rate ($Q \geq 3$) for 82 696 unique redshifts, 80 944 for the main survey (79 599 with $z > 0.002$). Table 4 gives a breakdown of the spectra obtained. Including spectra from other surveys, results in 100 012 $Q \geq 3$ redshifts for the main survey (98 497 with $z > 0.002$). Table 5 gives the target numbers and redshift completeness for various main survey selections. Note particularly the drop in completeness between $r_{petro} < 19.0$ (96 per cent average completeness) and the fainter r-band selection (74 per cent), and a further drop to the z- and K-band extra selection (39 per cent). The r-limit only selection and the prioritization in the first year is the main cause of differing $Q \geq 3$ completeness factors between each subsample, i.e. it is primarily a variation in targeting completeness though redshift success rate is also lower for the fainter samples. No observations based on J- and/or K-band photometry were started in the first year so the marginally resolved sample within each magnitude range is also of lower completeness.

The details of spectroscopic data reduction, including new defringing and sky-subtraction techniques, redshifting, comparison with other spectra, spatial and magnitude completeness will be described in future GAMA papers. In the next section, we use the first-pass redshifts to illustrate some issues related to the target selection.

5 RESULTS

5.1 Star–galaxy separation

There are two star–galaxy separation parameters used in the GAMA selection. Fig. 12(a) shows the observed bivariate distribution of main survey targets in these parameters. The red line shows the cut used for our target selection. This removes nearly 9000 sources or about 7 per cent of potential targets to $\Delta_{sg} > 0.05$. Figs 12(b) and (c) show the distributions of galaxies ($z > 0.002$) and stars that have confirmed redshifts, 1.5 per cent are stellar, using all available spectroscopic data. The additional $J - K$ selection was necessary for sources with $r > 17.8$ in order to be complete for compact galaxies. This is seen by the confirmed galaxy contours extending to the left of $\Delta_{sg} = 0.25$ in Fig. 12(b), which would otherwise have been missed by using only a $\Delta_{sg} > 0.25$ cut. Note that the targeting completeness is lower at $\Delta_{sg} < 0.25$, 60 per cent compared to nearly 90 per cent overall, because this UKIDSS–SDSS selection was not available for AAT observations in 2008.

Fig. 12 also shows that the regions of high stellar contamination are, not surprisingly, at low Δ_{sg} or $\Delta_{sg,jk}$. Thus a lower

Table 5. Main survey target numbers and redshift completeness for the three separate GAMA regions, galaxy fractions (from $Q \geq 3$ redshifts), and median galaxy redshifts. The redshift completeness is defined as the number of objects with a $Q \geq 3$ redshift divided by the number of targets (regardless of whether they have been observed spectroscopically).

Selection	Region G09		Region G12		Region G15		fraction	median
	Number of targets	$Q \geq 3$ (per cent)	Number of targets	$Q \geq 3$ (per cent)	Number of targets	$Q \geq 3$ (per cent)	$z > 0.002$ (per cent)	redshift
$r_{petro} < 16.0$	363	95.0	397	97.5	481	96.9	99.1	0.052
$16.0 < r_{petro} < 17.8$	3 335	99.2	4 644	99.3	4 666	99.0	98.5	0.116
$17.8 < r_{petro} < 19.0$ and $\Delta_{sg} > 0.25$	14 387	98.2	15 599	96.1	16 016	93.1	99.0	0.185
$17.8 < r_{petro} < 19.0$ and $\Delta_{sg} < 0.25$	160	83.8	206	60.7	153	55.6	66.3	0.260
$19.0 < r_{petro} < 19.4$ and $\Delta_{sg} > 0.25$	11 886	90.6	11 600	76.4	11 724	62.6	98.9	0.243
$19.0 < r_{petro} < 19.4$ and $\Delta_{sg} < 0.25$	201	77.1	345	46.1	223	33.6	80.7	0.228
$19.4 < r_{petro} < 19.8$ and $\Delta_{sg} > 0.25$	–	–	17 281	70.1	–	–	99.5	0.263
$19.4 < r_{petro} < 19.8$ and $\Delta_{sg} < 0.25$	–	–	853	38.9	–	–	93.7	0.254
$z_{model} < 18.2$ and not r selected	604	63.1	270	25.2	510	38.2	58.4	0.470
$K_{AB,auto} < 17.6$ and not rz selected	1 931	46.5	348	19.0	1 669	29.5	97.3	0.368
All main survey	32 867	91.6	51 543	80.9	35 442	79.5	98.5	0.196

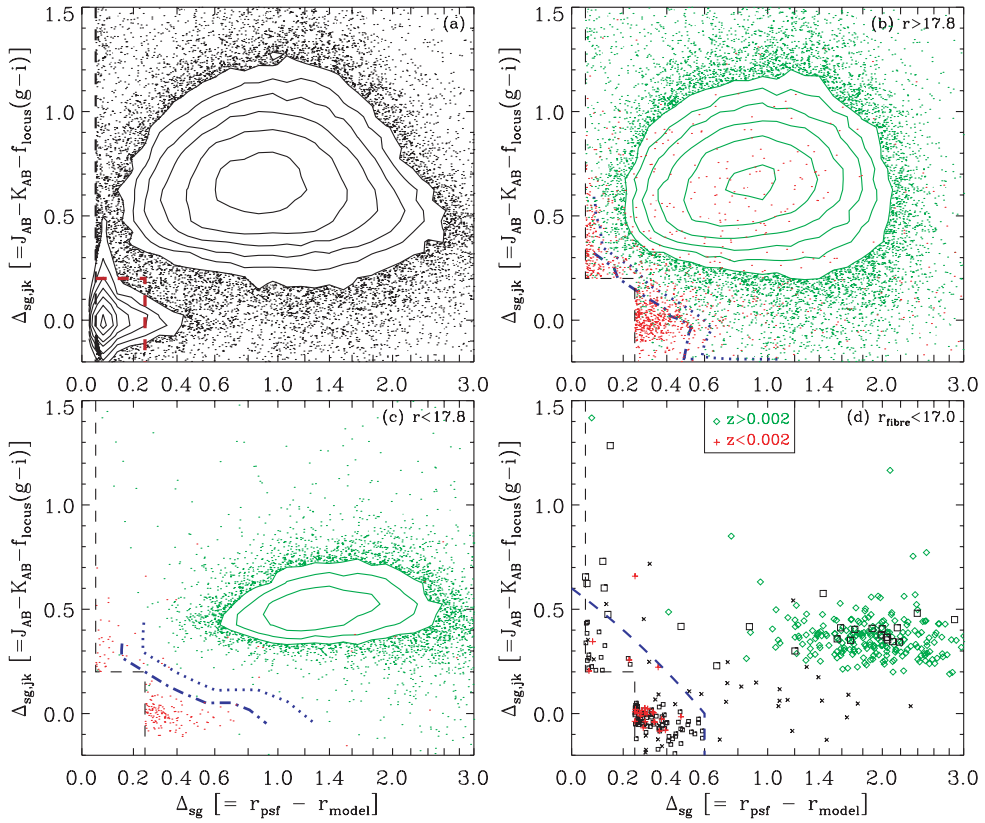

Figure 12. Results of star–galaxy separation. (a) The distribution of main survey targets with a $J - K$ measurement, extended to all objects with $\Delta_{sg} > 0.05$, are shown with black contours and points. The red dashed line shows the cut used for target selection. (b) and (c) The distribution of objects ($r_{petro} > 17.8$, < 17.8) with confirmed galaxy redshifts are shown with green contours and points, while objects with stellar redshifts are shown with red points. The blue dotted (dash–dotted) line corresponds to 50 per cent (70 per cent) stellar contamination for objects on or near the line (determined by interpolation in the $r < 17.8$ sample). (d) Objects with $r_{fibre} < 17.0$, not included in the AAOmega observation schedule, are shown. Red crosses and green diamonds represent objects with confirmed stellar and galaxy redshifts. Black crosses (squares) represent objects where the fibre magnitude is brighter (fainter) than the Petrosian magnitude. The smaller squares and crosses are the potential targets excluded by the criteria of equation (12): these are also shown as small red circles in Fig. 11. The blue dashed line divides the small and large squares.

contamination could be obtained by using a cut $\Delta_{sg} + \Delta_{sg,jk} > 0.4$, for example, with minimal rejection of genuine galaxies. This would work well because there is no strong correlation between the two parameters.

An estimate of the completeness of the current selection in terms of selecting galaxies can be obtained by assuming that there is no significant correlation between Δ_{sg} and $\Delta_{sg,jk}$. Consider the galaxy distribution in Fig. 12(b). The fraction of galaxies at $\Delta_{sg,jk} < 0.2$ is 2.3 per cent (not including galaxies with no $J - K$ measurement) and the fraction at $\Delta_{sg} < 0.25$ is 1.7 per cent after adjusting the latter for the lower targeting completeness. Thus the predicted fraction of galaxies at $\Delta_{sg,jk} < 0.2$ and $\Delta_{sg} < 0.25$ (in the lower left-hand corner of the plot) is only 0.04 per cent. Thus, the galaxy selection from the star–galaxy separation is plausibly $\gtrsim$99.9 per cent complete when there are J and K measurements. This assumes there is no significant population of galaxies with $\Delta_{sg} < 0.05$ within our magnitude limits.

The SDSS pipeline PHOTO also determines the scale radii of the de Vaucouleurs and exponential profile fits (equations 9 and 10 of Stoughton et al. 2002). Taking the best fit and averaging the scale radii in the r and i bands for each galaxy, we determined the completeness in this measure of size. The cut $\Delta_{sg} > 0.25$ is complete down to a scale radius ∼0.6 arcsec, while our star–galaxy separation (equation 5) is plausibly complete down to a scale radius ∼0.25 arcsec.[5] Fig. 13 shows the scale radius in kpc versus redshift for confirmed galaxies in the main survey. Without the additional selection, the target selection would be significantly incomplete, ∼20 per cent missed, for galaxies with observed radii between 0.25 and 0.6 arcsec. Of course, one could have used this scale radius directly as a star–galaxy separation parameter but, without higher resolution imaging, the systematic errors are presumably larger in this than Δ_{sg}.

This compact galaxy selection is critical for studies with a direct interest in the size evolution of galaxies (e.g. Trujillo et al. 2006; Cameron & Driver 2007; Taylor et al. 2009). Targeting all objects with $\Delta_{sg} > 0.05$ would have resulted in ∼9000 extra objects, which would have been a very inefficient way to target compact galaxies. Future higher S/N and higher resolution imaging (optical and near-IR) will improve the efficiency of this type of selection, providing

[5] We note that the PHOTO scale radius values should be interpreted with some caution at small sizes, less than half the typical PSF width. Taylor et al. (2009) advocate treating objects with scale radii <0.75 arcsec as having an upper limit of 0.75 arcsec, i.e. the true value is poorly determined even though PHOTO has determined that the object is likely to be resolved.

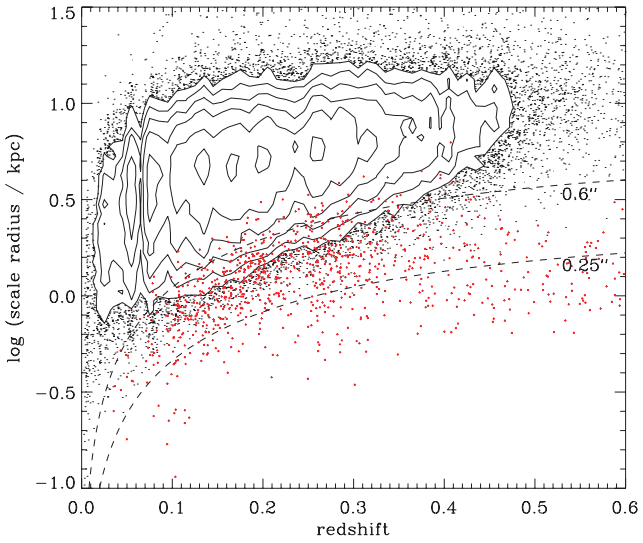

Figure 13. Scale radius, de Vaucouleurs or exponential profile from PHOTO, versus redshift. The black contours and points represent galaxies selected using $\Delta_{sg} > 0.25$, while red crosses represent the $J - K$ selected sample with $0.05 < \Delta_{sg} < 0.25$. The dashed lines correspond to constant observed angular size.

a test of whether GAMA target selection has missed significant numbers of compact galaxies.

5.2 Bright galaxies

Objects with $r_{\rm fibre} < 17.0$ are not allocated to the AAOmega schedule to avoid cross-talk between spectra tramlines, and we do not need to consider these objects for this target selection. However, it is necessary for analyses at low redshift, e.g. measuring luminosity functions, to determine a realistic completeness of galaxy selection at bright magnitudes. Fig. 12(d) shows the distribution in the star–galaxy separation parameters for these potential targets. There are 485 using our normal selection criteria, of which, 296 have redshifts from SDSS and other surveys ($Q \geq 3$; Table 3). One possibility would be to observe all remaining 189 targets with a 2-m-class telescope. However, most of these are probably stars and a more restrictive criterion could be used. This is given by

$$r_{\rm fibre} > 17.0$$
or
$$(\Delta_{sg} + \Delta_{sg,jk} > 0.6 \text{ or } \Delta_{sg} > 0.6$$
and
$$r_{\rm fibre} > r_{\rm petro}). \quad (12)$$

The Δ_{sg}–$\Delta_{sg,jk}$ cut is shown by the blue dashed line in Fig. 12(d), while targets that satisfy the last criteria are shown as squares as opposed to crosses. Sources with fibre magnitude brighter than Petrosian are indicative of a 'possible' galaxy blended with a star; however, the starlight dominates the fibre magnitude, which is not deblended. Using the above cut results in 299 sources with 266 redshifts (89 per cent complete). This cut should be used when assessing completeness at the bright end of GAMA targets. This was applied before computing the $r_{\rm petro} < 16$ target numbers and completeness given in Table 5.

5.3 Low surface brightness galaxies

The completeness in the low-SB regime depends on redshift success and source detection (Disney & Phillipps 1983; Blanton et al. 2005), and there is the additional issue of the accuracy of the flux measurements (Cameron & Driver 2007). These will be described in detail in a future paper on luminosity functions (Loveday et al., in preparation). Here we note only that the redshift success rate is primarily a function of $r_{\rm fibre}$ as shown in Fig. 11. The success rate is 50 per cent at $r_{\rm fibre} \sim 21.5$. This does not include any coadding of GAMA spectra over two or more observations, and there may be improvement after re-reduction.

5.4 Redshift distributions and near-IR selections

Not accounting for incompleteness, 50 per cent of the galaxy redshifts are in the range of 0.13–0.27, 90 per cent are in the range of 0.06–0.39 and 99 per cent are in the range of 0.02–0.53. Fig. 14 shows the redshift histograms for various galaxy samples ($z > 0.002$) within the main survey, and median redshifts are given in Table 5. The near-IR selections have a higher average redshift. Note that the redshift distribution within each subsample may be biased by non-GAMA redshifts and the dependence of redshift success rate on magnitude, for example. These are corrected for in Fig. 14 by binning in $g - i$ to determine completeness factors. The histogram for each subsample is determined by weighting each object with a redshift by $1/c$, where c is the redshift completeness in each bin (with bin size of 0.2 for $0 < g - i < 3$). This colour is used because of its correlation with redshift (Fig. 6b).

Fig. 15(a) shows observed $r - z$ versus redshift for the z-selected sample, with the targets fainter than 19.4 in r shown by red points. The extra z-band selection is mostly picking up luminous galaxies in the redshift range of 0.4–0.6 (recalling that this is of lower completeness than the $r < 19.4$ selection). The number density of targets drops off well before the colour bias limit. Simple stellar population (SSP) tracks are shown with a formation redshift of six (see caption for references). Some objects are apparently redder than the old SSP tracks. This is presumably mostly because of photometric errors; however, certain dust geometries can in principle redden galaxies beyond the colour of old stellar populations. Dusty galaxies can lie on, and slightly redder than, the red sequence (Wolf,

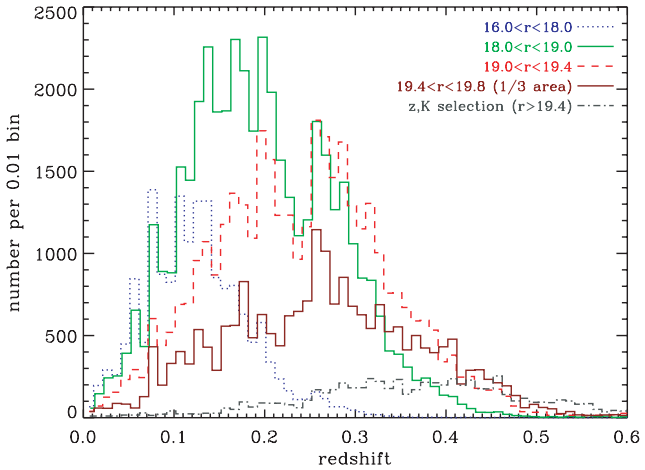

Figure 14. Redshift distributions for selected main-survey samples. The numbers have been projected to completion of the main survey using empirical completeness determined in $g - i$ bins.

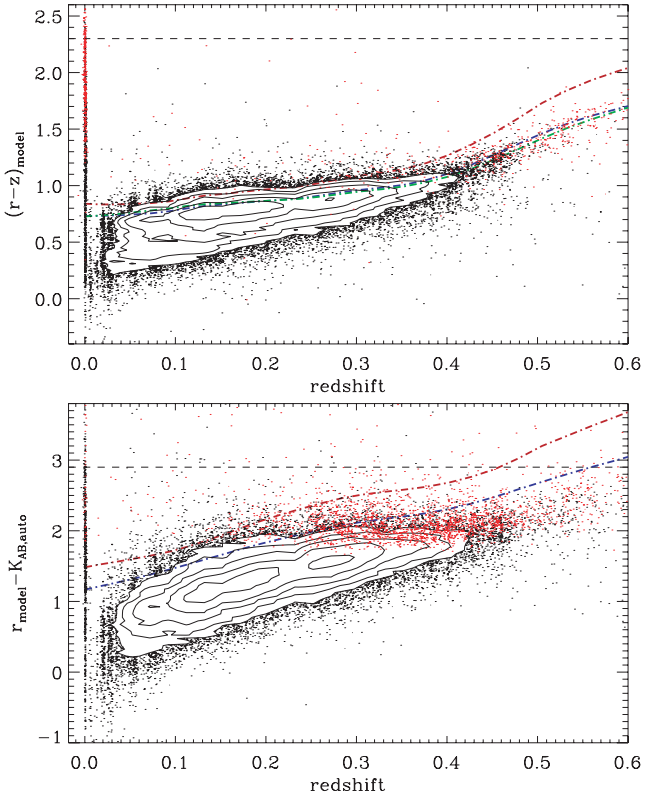

Figure 15. Observed colour versus redshift for (a) the $z_{\rm model} < 18.2$ sample and (b) the $K_{\rm AB,auto} < 17.6$ sample. The black contours and points represent the data within $r_{\rm petro} < 19.4$ (or $z_{\rm model} < 18.2$ for the K-selected sample), while the red points represent the remaining fainter selection. The dash–dotted lines represent the observed colours of SSP models with $z_{\rm form} = 6$ (12.5-Gyr old at $z = 0$, 7.5 Gyr at $z = 0.5$): red ($Z = 0.05$; Bruzual & Charlot 2003), blue ($Z = 0.04$, alpha-enhanced abundances; Percival et al. 2009) and green ($Z = 0.02$, empirical stellar spectra; Maraston et al. 2009). The horizontal dashed line represents the completeness limit at the faint end of the samples given the $r_{\rm model} < 20.5$ limit (Fig. 10).

Gray & Meisenheimer 2005). Note that most of the targets in the range $1.2 < r - z < 2.5$ are a stellar contamination (or 41.6 per cent of the z-band extra selection; see Table 5).

Fig. 15(b) shows observed $r_{\rm model} - K_{\rm AB,auto}$ versus redshift for the K-selected sample, with the targets fainter than 19.4 in r and 18.2 in z shown by red points. The extra selection is mostly picking up red galaxies in the redshift range of 0.2–0.5. The tracks show that the K selection is possibly incomplete for maximally old supersolar metallicity populations at redshift >0.45 (from one of the models). There are many sources significantly redder than the tracks; however, this is most probably because of the mismatch in apertures between the surveys (model versus AUTO mags, different deblending algorithms). For most purposes, it would be adequate to assume that the selection is K-band limited only.

6 SUMMARY

The GAMA survey is designed to be a highly complete redshift survey with a target density several times that of SDSS. The survey covers three 48 deg^2 regions near the celestial equator centred on 9, 12 and 14.5 h (Fig. 2). The input catalogue is drawn from the SDSS and UKIDSS. The main-survey limits are $r_{\rm petro} < 19.4$, $z_{\rm model} < 18.2$ and $K_{\rm AB,auto} < 17.6$ ($K < 15.7$) across all the regions, and $r_{\rm petro} < 19.8$ over the G12 region (equation 6). This corresponds to a main survey of 119 852 targets. The near-IR selections have a joint constraint with $r_{\rm model} < 20.5$, which has minimal impact on the use of the near-IR selections (Figs 10 and 15). The GAMA survey lies between that of the SDSS-MGS $r < 17.8$ and VVDS-wide $I_{\rm AB} < 22.5$ magnitude-limited samples in the depth-area plane (Fig. 1). In terms of K-band selection (Figs 3 and 4), GAMA covers an area ∼15 times that of the similar-depth Hawaii+AAO $K < 15$ survey.

In order to be highly complete at the high-SB end of the galaxy distribution, an intensity profile parameter (equation 1) and a colour–colour parameter (equation 2) are used jointly for star–galaxy separation. The $\Delta_{\rm sg,jk}$ parameter makes use of $J - K$ and $g - i$ colours. Either parameter works reasonably well in separating stars and galaxies (Figs 5–8). A joint selection (equation 5) increases the completeness while stellar contamination in the sample remains at less than 2 per cent. Judging by the joint distribution of confirmed galaxies in these parameters (Fig. 12), the completeness is high because the bivariate density drops significantly prior to the limit of our selection. This is particularly important when considering the size evolution of galaxies (Fig. 13). The incompleteness at the low-SB end is significant, both in source detection and redshift success rate, which is about 50 per cent at $r_{\rm fibre} = 21.5$ (Fig. 11). Some improvement over the SDSS MGS is made by visually checking low-SB targets ($\mu_{r,50} > 23$), rather than using automatic checks, by increased redshift success rate, and by eventually including further integrations of sources with failed redshifts.

The GAMA survey has completed two out of a 3-yr time allocation for spectroscopy with AAOmega on the AAT. To date, 100 012 redshifts have been confirmed for the main survey, including 80 944 from AAOmega. Of these, 98.5 per cent are extragalactic. The completeness is 96 per cent for $r_{\rm petro} < 19.0$, 74 per cent for the fainter r-band selection, and ∼39 per cent for the remaining near-IR selection (Table 5). The completeness at $r > 19$ will be significantly improved in the third year of spectroscopic observations. We expect that this galaxy redshift survey will form a core of a fundamental data base for many studies in extragalactic astronomy.

ACKNOWLEDGMENTS

This part of the GAMA survey has been made possible by the efforts of staff at the Anglo-Australian Observatory, and members of the Sloan Digital Sky Survey and UKIRT Infrared Deep Sky Survey teams. We thank Steven Warren in particular for efforts in making the GAMA regions a high priority in UKIDSS, the anonymous referee for useful suggestions and Daniel Mortlock for discussion regarding star–galaxy separation. Data base and software resources used in this paper include the SDSS Catalog Archive Server Jobs (CASJobs) System, the UKIDSS WFCAM Science Archive (WSA), the VizieR catalogue service, the IDL Astronomy User's Library, IDLUTILS, Astromatic software and Starlink Tables Infrastructure Library Tool Set (STILTS). IB acknowledges funding from Science and Technology Facilities Council (STFC) and Higher Education Funding Council for England (HEFCE).

REFERENCES

Abazajian K. et al., 2004, AJ, 128, 502
Abazajian K. et al., 2009, ApJS, 182, 543
Adelman-McCarthy J. K. et al., 2006, ApJS, 162, 38
Adelman-McCarthy J. K. et al., 2008, ApJS, 175, 297
Berlind A. A. et al., 2006, ApJS, 167, 1
Bertin E., Arnouts S., 1996, A&AS, 117, 393

Bertin E., Mellier Y., Radovich M., Missonnier G., Didelon P., Morin B., 2002, in Bohlender D. A., Durand D., Handley T. H., eds, ASP Conf. Ser. Vol. 281, ADASS XI. Astron. Soc. Pac., San Francisco, p. 228
Binggeli B., Sandage A., Tammann G. A., 1988, ARA&A, 26, 509
Blanton M. R. et al., 2003, ApJ, 592, 819
Blanton M. R., Lupton R. H., Schlegel D. J., Strauss M. A., Brinkmann J., Fukugita M., Loveday J., 2005, ApJ, 631, 208
Bruzual G., Charlot S., 2003, MNRAS, 344, 1000
Cameron E., Driver S. P., 2007, MNRAS, 377, 523
Cannon R. et al., 2006, MNRAS, 372, 425
Carlberg R. G., Yee H. K. C., Ellingson E., Abraham R., Gravel P., Morris S., Pritchet C. J., 1996, ApJ, 462, 32
Casali M. et al., 2007, A&A, 467, 777
Cole S. et al., 2001, MNRAS, 326, 255
Colless M. et al., 2001, MNRAS, 328, 1039
Colless M. et al., 2003, preprint (astro-ph/0306581)
Cotton W. D., Condon J. J., Arbizzani E., 1999, ApJS, 125, 409
Croom S., Saunders W., Heald R., 2004a, Anglo-Australian Obser. Newslett., 106, 12
Croom S. M., Smith R. J., Boyle B. J., Shanks T., Miller L., Outram P. J., Loaring N. S., 2004b, MNRAS, 349, 1397
Croom S. M. et al., 2009, MNRAS, 392, 19
da Costa L. N. et al., 1998, AJ, 116, 1
Davis M., Geller M. J., Huchra J., 1978, ApJ, 221, 1
Davis M., Huchra J., Latham D. W., Tonry J., 1982, ApJ, 253, 423
Davis M. et al., 2003, Proc. SPIE, 4834, 161
de Lapparent V., Geller M. J., Huchra J. P., 1988, ApJ, 332, 44
De Propris R., Liske J., Driver S. P., Allen P. D., Cross N. J. G., 2005, AJ, 130, 1516
Disney M., Phillipps S., 1983, MNRAS, 205, 1253
Drinkwater M. J. et al., 2010, MNRAS, 401, 1429
Driver S. P., Liske J., Cross N. J. G., De Propris R., Allen P. D., 2005, MNRAS, 360, 81
Driver S. P. et al., 2009, Astron. Geophys., 50, 5.12
Dye S. et al., 2006, MNRAS, 372, 1227
Eisenstein D. J. et al., 2001, AJ, 122, 2267
Eke V. R. et al., 2004, MNRAS, 348, 866
Eke V. R., Baugh C. M., Cole S., Frenk C. S., Navarro J. F., 2006, MNRAS, 370, 1147
Ellis R. S., Colless M., Broadhurst T., Heyl J., Glazebrook K., 1996, MNRAS, 280, 235
Elston R. J. et al., 2006, ApJ, 639, 816
Erdoğdu P. et al., 2006, MNRAS, 368, 1515
Falco E. E. et al., 1999, PASP, 111, 438
Fukugita M., Ichikawa T., Gunn J. E., Doi M., Shimasaku K., Schneider D. P., 1996, AJ, 111, 1748
Garilli B. et al., 2008, A&A, 486, 683
Gunn J. E. et al., 1998, AJ, 116, 3040
Hambly N. C. et al., 2008, MNRAS, 384, 637
Hewett P. C., Warren S. J., Leggett S. K., Hodgkin S. T., 2006, MNRAS, 367, 454
Hodgkin S. T., Irwin M. J., Hewett P. C., Warren S. J., 2009, MNRAS, 394, 675
Hogg D. W., Finkbeiner D. P., Schlegel D. J., Gunn J. E., 2001, AJ, 122, 2129
Huang J.-S., Glazebrook K., Cowie L. L., Tinney C., 2003, ApJ, 584, 203
Huchra J. P., Geller M. J., 1982, ApJ, 257, 423
Ivezić Ž. et al., 2002, in Green R. F., Khachikian E. Y., Sanders D. B., eds, ASP Conf. Ser. Vol. 284, AGN Surveys. Astron. Soc. Pac., San Francisco, p. 137
Jarrett T. H., Chester T., Cutri R., Schneider S., Skrutskie M., Huchra J. P., 2000, AJ, 119, 2498
Jarrett T. H. et al. 2010, AJ, submitted
Jones D. H. et al., 2009, MNRAS, 399, 683
Kniazev A. Y., Grebel E. K., Pustilnik S. A., Pramskij A. G., Kniazeva T. F., Prada F., Harbeck D., 2004, AJ, 127, 704
Kron R. G., 1980, ApJS, 43, 305
Lawrence A. et al., 2007, MNRAS, 379, 1599
Le Fèvre O. et al., 2005, A&A, 439, 845
Lewis I. J. et al., 2002, MNRAS, 333, 279
Lilly S. J., Le Fevre O., Crampton D., Hammer F., Tresse L., 1995, ApJ, 455, 50
Lilly S. J. et al., 2007, ApJS, 172, 70
Liske J., Lemon D. J., Driver S. P., Cross N. J. G., Couch W. J., 2003, MNRAS, 344, 307
Loveday J., Peterson B. A., Efstathiou G., Maddox S. J., 1992, ApJ, 390, 338
MacGillivray H. T., Martin R., Pratt N. M., Reddish V. C., Seddon H., Alexander L. W. G., Walker G. S., Williams P. R., 1976, MNRAS, 176, 265
Maddox S. J., Efstathiou G., Sutherland W. J., Loveday J., 1990, MNRAS, 243, 692
Maraston C., Strömbäck G., Thomas D., Wake D. A., Nichol R. C., 2009, MNRAS, 394, L107
Moore B., Frenk C. S., White S. D. M., 1993, MNRAS, 261, 827
Norberg P. et al., 2002a, MNRAS, 332, 827
Norberg P. et al., 2002b, MNRAS, 336, 907
Padmanabhan N. et al., 2008, ApJ, 674, 1217
Percival S. M., Salaris M., Cassisi S., Pietrinferni A., 2009, ApJ, 690, 427
Peterson B. A., Ellis R. S., Efstathiou G., Shanks T., Bean A. J., Fong R., Zen-Long Z., 1986, MNRAS, 221, 233
Ratcliffe A., Shanks T., Broadbent A., Parker Q. A., Watson F. G., Oates A. P., Fong R., Collins C. A., 1996, MNRAS, 281, L47
Robotham A. et al., 2009, Publ. Astron. Soc. Australia, in press (arXiv:0910.5121)
Saunders W., Rowan-Robinson M., Lawrence A., Efstathiou G., Kaiser N., Ellis R. S., Frenk C. S., 1990, MNRAS, 242, 318
Saunders W. et al., 2000, MNRAS, 317, 55
Saunders W., Cannon R., Sutherland W., 2004, Anglo-Australian Obser. Newslett., 106, 16
Schechter P., 1976, ApJ, 203, 297
Schlegel D. J., Finkbeiner D. P., Davis M., 1998, ApJ, 500, 525
Sharp R. et al., 2006, Proc. SPIE, 6269, 62690G
Shectman S. A., Landy S. D., Oemler A., Tucker D. L., Lin H., Kirshner R. P., Schechter P. L., 1996, ApJ, 470, 172
Skrutskie M. F. et al., 2006, AJ, 131, 1163
Smith J. A. et al., 2002, AJ, 123, 2121
Steidel C. C., Adelberger K. L., Shapley A. E., Pettini M., Dickinson M., Giavalisco M., 2003, ApJ, 592, 728
Stoughton C. et al., 2002, AJ, 123, 485
Strauss M. A. et al., 2002, AJ, 124, 1810
Taylor M. B., 2005, in Shopbell P., Britton M., Ebert R., eds, ASP Conf. Ser. Vol. 347, ADASS XIV. Astron. Soc. Pac., San Francisco, p. 29
Taylor E. N., Franx M., Glazebrook K., Brinchmann J., van der Wel A., van Dokkum P. G., 2009, ApJ, submitted (arXiv:0907.4766)
Trujillo I. et al., 2006, ApJ, 650, 18
Vettolani G. et al., 1997, A&A, 325, 954
Warren S. J. et al., 2007, MNRAS, 375, 213
Watson C. R. et al., 2009, ApJ, 696, 2206
Wolf C., Gray M. E., Meisenheimer K., 2005, A&A, 443, 435
Yee H. K. C. et al., 2000, ApJS, 129, 475
York D. G. et al., 2000, AJ, 120, 1579
Zehavi I. et al., 2005, ApJ, 630, 1
Zwicky F., 1937, ApJ, 86, 217

This paper has been typeset from a TEX/LATEX file prepared by the author.